Polymer Testing 74 (2019) 266–273

Contents lists available at ScienceDirect

Polymer Testing

journal homepage: www.elsevier.com/locate/polytest

Material Properties

Effects of bulk viscoelasticity and surface wetting on the contact and adhesive properties of a soft material

Meng Li, Qing Jiao, Qingwen Dai, Liping Shi, Wei Huang, Xiaolei Wang*

National Key Laboratory of Science and Technology on Helicopter Transmission, Nanjing University of Aeronautics & Astronautics, Nanjing, 210016, China

ARTICLE INFO

Keywords:
Contact
Adhesion
Stick-split
Bulk viscoelasticity
Surface wetting

ABSTRACT

Because of the wide practical applications of soft materials, the surface contact and adhesive behaviors need to be comprehensively understood. Here, we systematically investigated the effect of bulk viscoelasticity and surface wetting on the dynamic behavior of contact and adhesion of soft polydimethylsiloxane (PDMS) surfaces. Experimental results showed that during the indentation process, the relation between loads and contact radius were close to the Johnson-Kendall-Roberts (JKR) mode, but the load-penetration curves presented a roughly linear dependence with increasing preloads transferring from the JKR to Hertz mode; the detaching process exhibited a pronounced "stick-split" behavior, where the spherical probe first stuck to the soft PDMS without decreasing the contact area, and then the crack of the contact edge opened and split, providing high adhesive forces far exceeding the JKR prediction. The introduction of liquids between the probe and soft PDMS strongly decreased the contact area, reduced the stick time, and weakened the dry adhesive strength depending on the surface tension. The internal friction induced by the segmental motion of long-chain molecules and the interfacial resistance of liquid were suggested to be responsible for these phenomena.

1. Introduction

Contact and adhesion of soft materials to wet surfaces are common but of significant importance in our daily life and the biological world. When driving on wet roads, the soft tires are desired to contact closely with the pavement to form a strong attachment to keep the car under control. Certain amphibians, such as tree frogs and newts, also utilize their soft toe-pads to achieve reliable adhesion on wet leaves or stones for foraging or defense in the rainforest [1–4]. Studying the mechanical interaction of elastically soft solids for adhesion is expected to notably contribute to our understanding of biological epidermal adhesion and facilitate major developments in some applied fields, e.g. soft robotics, traffic vehicles, and artificial adhesive surfaces.

Over the last decade, significant scientific attention has been paid to micro- and nanostructures for their interfacial adhesive properties, well revealing the design principle of surface topography for controllable adhesion on soft surfaces [5–7]. However, as a result of pluralistic interaction, the interfacial contact or adhesive is also influenced by other physical factors, e.g., inner bulk viscoelasticity [8,9] and surface wetting conditions [10–12]. Gent early pointed out that the adhesive strength of a soft surface is a combination of the intrinsic energy of the interface adhesion and the dissipated energy of bulk viscoelastic loss [9]. Such energy dissipation leads to significant adhesive hysteresis between the loading and unloading processes [13,14] An increase in pull-off speed [15–17] or decrease in polymer temperature [18] was suggested to increase the dissipated effect, producing the enhanced adhesive strength on a soft surface. On the other hand, if the contact of a soft material is wetted, the interfacial adhesive performance is also influenced by the presented liquid properties. Previous studies have demonstrated that there always is dry contact on polymer by dewetting behavior if the surficial liquid does not present a totally wetting case [11,12,19]. Unlike the dry case, the adhesive strength of this partial dry contact strongly depends on the interfacial drastic liquid–solid interaction [20–23].

Although many studies on adhesives have addressed the positive role of viscoelasticity for interfacial strength, experimental investigations on the dynamic behavior of contact and adhesion are relatively limited. Few of the existing studies quantitatively explored the viscoelastic response on the correlative characteristics of contact area, penetration depth, and contact/adhesion force of soft surfaces during the time-dependent indentation/detachment, as well as considering the presence of a surficial liquid. Furthermore, the normal Johnson-Kendall-Roberts (JKR) theory proposed for the dry pure elastomer seems to fail to accurately predict the adhesive behavior on a wet viscoelastic surface; as a result, relevant experimental studies are desired.

In this study, we experimentally investigated the effect of bulk

* Corresponding author.
E-mail address: wxl@nuaa.edu.cn (X. Wang).

https://doi.org/10.1016/j.polymertesting.2019.01.019
Received 31 October 2018; Received in revised form 20 January 2019; Accepted 22 January 2019
Available online 23 January 2019

viscoelasticity and surface wetting condition on the dynamic behavior of contact and adhesion between a spherical glass probe and soft polydimethylsiloxane (PDMS). The mechanical characteristics of interfacial force, penetration depth, and contact radius dependence of time during the loading and unloading processes were precisely investigated using an advanced micro-force tester, and compared with JKR theoretical predictions. A deionized water and ethanol solution was employed to study the effect of surface wetting on the adhesive characteristics of contact area, critical pull-off radius, and pull-off force on the soft PDMS surface. The obtained results provide a better understanding of the adhesive property of wet viscoelastic materials and help guide the design of adhesive tires for wet roads.

2. Experimental section

2.1. Sample fabrication

PDMS (Sylgard 184, Dow Corning) was conventionally mixed with a prepolymer to cross-linker ratio of 10:1. In addition, low-viscosity dimethyl silicone oil (PMX-200, viscosity 10cs, Dow Corning) was added into the PDMS mixture with a ratio of 0.5:1. Such fillers stretch the crosslinked network of PDMS, reduce the hardness, and increase the bulk viscoelasticity [11] (Fig. 1a). Then, the entire mixture was degassed and poured onto a prepared glass mold and cured at 70 °C for 12 h in a vacuum oven. After cooling to room temperature, the soft PDMS sample was carefully peeled from the mold.

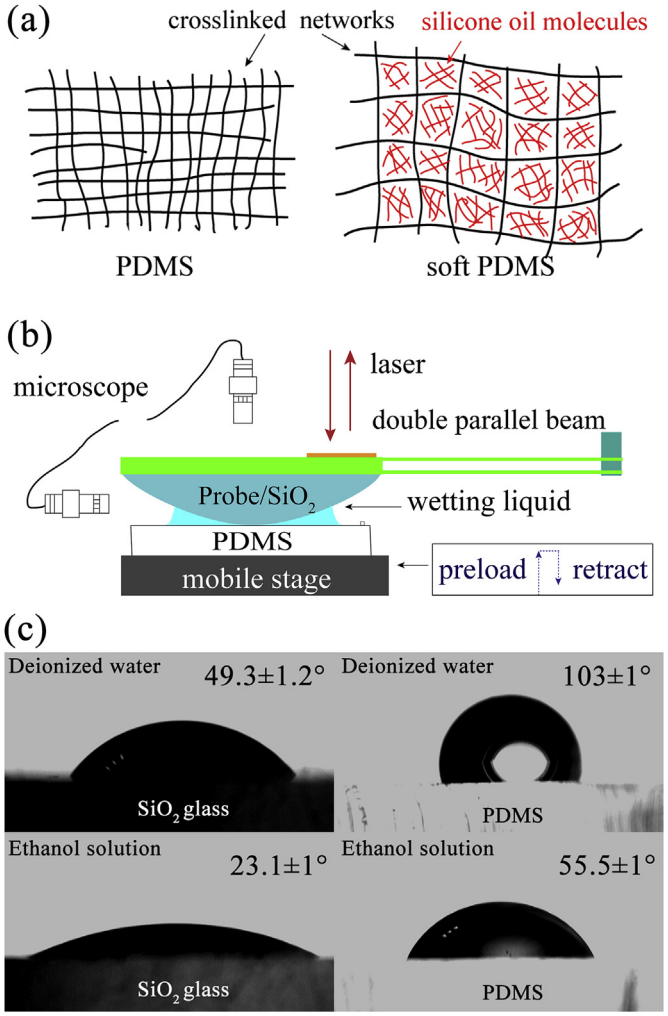

Fig. 1. (a) Schematic illustration of filling silicone oil for soft PDMS, (b) schematic illustration of the measurement setup, and (c) contact angles of deionized water and ethanol solution on SiO_2 glass and PDMS surface.

2.2. Indentation measurements

Indentation and adhesion measurements were both performed using a custom-made setup, as shown in Fig. 1b, which is described in detail elsewhere [24]. It consisted of a mobile stage composed of a piezo (P-611.3, Physik Instrumente, Germany), a step motor (Lianyi, China) and a flexible double parallel beam mounted with a glass probe. The probe here was a plano-convex lens with a curve radius of 18.5 mm (Purshee, China), Young's modulus of 7.2×10^{11} Pa, and Poisson's ratio of 0.2. The stiffness of the force-sensitive beam K was 509 N/m. The impress process was fully driven by the piezo at approximately 2 μm/s; the contact area at the interface between the SiO_2 probe and soft PDMS was monitored and recorded by an *in situ* microscopic visualization system.

The press-in depth of the probe on soft PDMS, δ, is usually calculated with the interaction force of cantilever F and the piezo distance Δ using the following relation [14]:

$$\delta = \Delta - \delta_m = (Z - Z_0) - \frac{F}{K} \quad (1)$$

where δ_m stands for the deflection of the cantilever beam, Z is the real-time position of the piezo, and Z_0 is the piezo position at the initial contact with the minimum detectable attractive force of the loading curve (i.e., immediately before the "jump-to-contact" region). Fig. 2 shows the representative curves of piezo distance, press-in depth, and interacted force versus time in indentation measurements at preload values of 4 mN and 6 mN. All these recorded values show an obvious linear correction to time, keeping a constant slope, i.e., the same rate in indentations, independent of preloads. Note that the regions inside the circles in the captured images are the contacts between the probe and the PDMS surface, and the dark regions are shadows induced by uneven illumination.

2.3. Adhesion measurements

Deionized water and an ethanol solution [50%(v/v)] were used to wet the soft PDMS surface for adhesion tests. The surface tensions of these two liquids at 25 °C are 72.35 ± 0.22 mN/m and 27.38 ± 0.1 mN/m, and their contact angles on soft PDMS are shown in Fig. 1c. For wet adhesion measurements, a liquid drop of 3 μL was first placed on the soft PDMS surface using a micropipette, and located on the center below the probe under the control of the microscope system. Measurements were then performed with the probe approaching, indenting, standing, and retracting. Fig. 3 shows the representative force-time curves with corresponding images of contact status measured in the dry, water, and ethanol-solution cases. With regard to the pull-off behavior in the presence of liquids, the adhesive force obviously exhibits two components: dry detachment and capillary interaction [11]. For retractions, the piezo first moved at a speed of 1 μm/s to conduct the short-range dry detachment event, and when beyond the piezo range (100 μm), a step motor launched at a speed of 10 μm/s to break the long-range capillary interaction. For dry adhesion measurements, the retraction for divorce was driven only by the piezo. The contact boundaries were not clear in the presence of liquids, which are marked with dashed lines in Fig. 3 b and c. The entire measurement process was recorded by a force sensor and monitored using an optical camera. The test for each sample was performed at least five times.

3. Results

3.1. Hertz mode or JKR mode of the indentation on soft PDMS?

Fig. 4a shows the force-penetration curves of probe indentation on soft PDMS with varying preloads. It can be seen that from the original point where the probe just touches the polymer surface to the zero

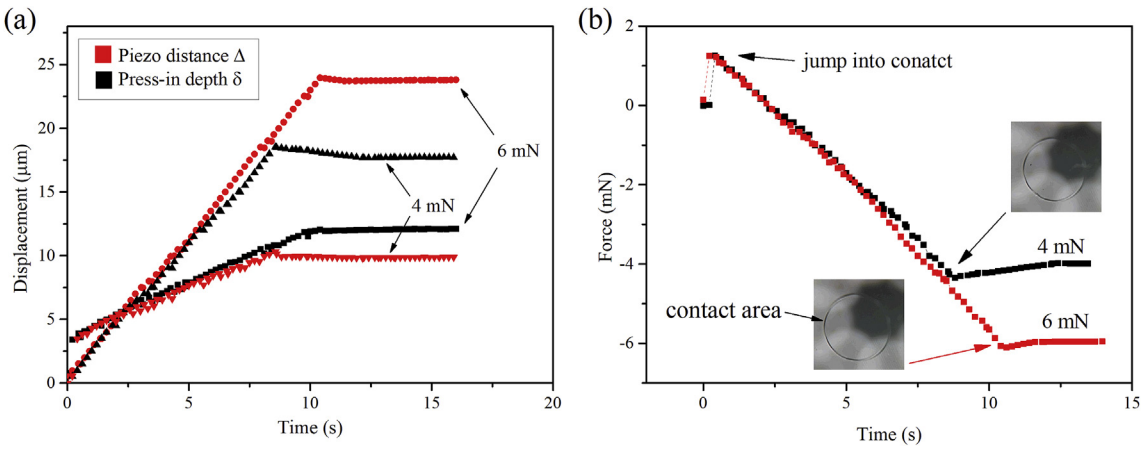

Fig. 2. (a) Piezo distance and press-in depth and (b) the relevant interfacial force interaction versus time at preload values of 4 mN and 6 mN. The velocity of the piezo for indentation was approximately 2 μm/s. The circular regions in the captured images are the contacts; the dark regions are shadows induced by uneven illumination.

points of the force curves, the indentation processes are dominated by an adhesive regime giving almost the same maximum attractive forces of about 1.24 mN. The plotted symbols for the indentation process with various loads interweave and overlap, generally presenting a linear dependence. For visualized comparison, the Hertz and JKR models are also both depicted in Fig. 4a using equations (2) and (3), respectively [25,26]:

$$F = \frac{4}{3}E^{*}R^{\frac{1}{2}}\delta^{\frac{3}{2}},\ a = \left(\frac{3FR}{4E^{*}}\right)^{\frac{1}{3}} \tag{2}$$

$$\begin{cases} a^3 = \frac{3R}{4E^{*}}\left(F + 3\Delta\gamma\pi R + \sqrt{6\Delta\gamma R\pi F + (3\Delta\gamma\pi R)^2}\right) \\ \delta = \frac{a^2}{3R} + \frac{F}{2aE^{*}} \end{cases} \tag{3}$$

where R is the probe radius, F is the applied load, a is the contact radius, δ is the indentation depth, E^{*} is the effective elastic modulus, and $\Delta\gamma$ is the work of adhesion. The apparent elastic modulus of this soft PDMS was 0.6 MPa [11], and the work of adhesion was approximately 25 mJ/m^2 [estimated by JKR theory at the zero point of the force-depth curve (Fig. 4a)]. It was found that the experimental force-penetration curves perform an obvious transformation from JKR to Hertz indentation depending on the preload. At light indentations, the symbols of force-penetration distribute around the JKR line, whereas at heavy indentations, the symbols shift to the Hertz line. Fig. 4b represents the contact radius captured between the probe and soft PDMS versus time corresponding to the indentation process of Fig. 4a, and the theoretical contact radius of Hertz and JKR are also provided. The measured contact radius increases with increasing preload in the indentations, and their symbol lines versus time also interweave and overlap, approaching the theoretical line calculated by JKR.

3.2. Stick-split behavior characterizing the adhesion of soft PDMS surface

Fig. 5a shows a specific force-penetration curve of retraction obtained at a preload of 2 mN and velocity of 0.25 μm/s (the JKR mode is also provided for comparison). A is the starting point of retraction, where the indentation of soft PDMS is 7.8 μm at a preload of 2 mN; B is the highest pull-off force point with a value of approximately 17 mN, far exceeding the JKR prediction. Between the indentation and retraction processes, a hysteresis is found. In examining the characteristics of the force-penetration curve of retraction, it seems to comprise two parts: the initial linear and then a nonlinear correlation. From previous studies [26], the linear force-depth dependence ($F \propto \delta$) was usually characterized by a flat-punch indentation, meaning that a constant contact area between the probe and soft PDMS here imposed on retraction. The *in situ* visualizations of contact radius in Fig. 5b further verify this assumption. From the point A to the critical point of linearity to nonlinearity, the contact radius remained constant, implying the soft PDMS strongly stuck the probe without splitting; after that critical point, the contact edge opened and receded slowly at first, then rapidly until the total separation of C, leaving a distinct mark on the soft PDMS (see captured image in Fig. 5b). These pull-off behaviors reflected the

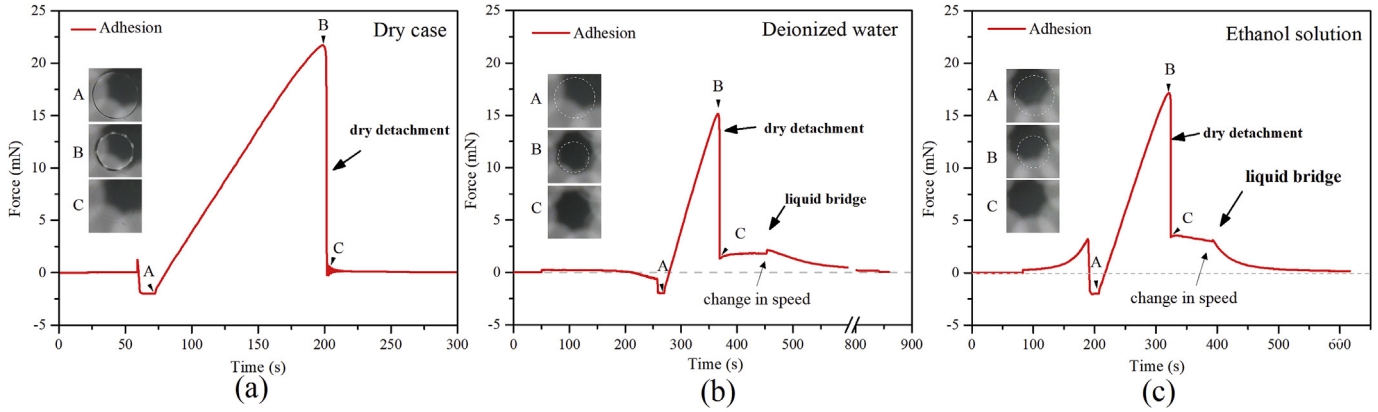

Fig. 3. Measured force curves in real time with corresponding images of contact area in different interfacial contact cases: (a) Dry, (b) deionized water, and (c) ethanol solution. A is the contact image when the detachment begins; B is the critical contact image at the time the adhesive force is recorded; and C is the contact image after the dry detachment. The contact boundaries in the presence of deionized water and ethanol solution are marked with dashed lines.

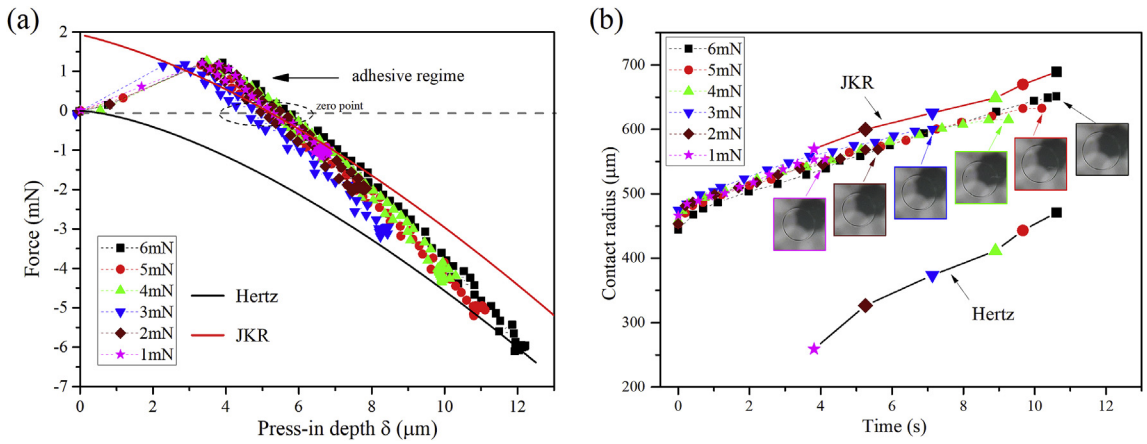

Fig. 4. Results of indentation measurements of a SiO_2 probe on soft PDMS in the dry case: (a) Force-depth curves and (b) the corresponding contact radius versus time depending on preload. The apparent elastic modulus of this soft PDMS was 0.6 MPa, and the work of adhesion was estimated as 25 mJ/m^2.

"stick-split" characteristic on the detachment of the soft PDMS surface, similar to the "stick-slip" of the frictional sliding on a polymer surface.

Fig. 5c shows the piezo distance Δ (red line) and the press-in depth (black line) versus time corresponding to the indentation and retraction process in Fig. 5a. The press-in depth versus time in retraction was also characterized by two correlations: linearity and nonlinearity, synchronizing with the force-penetration curve (Fig. 5a). In the nonlinear region, the highest pull-off force point B is marked and its tangent is drawn with fine red line. It was found that the tangent line at B was parallel to the red retraction line, signifying that in retraction, the highest pull-off force was achieved at the point where the stretch rate of soft PDMS reached the velocity of the piezo.

3.3. Effect of liquids on the adhesive property of soft PDMS surface

Fig. 6a shows the detected contact radius (A point in Fig. 3) as a function of preload with different surface wetting conditions. For all wetting cases, the contact radius increased with increasing preload. At the same preload, the introduced liquids strongly decreased the contact radius with dependence of surface tension. The critical pull-off contact radius between the probe and soft PDMS (the highest pull-off force point of B in Fig. 3) in different wetting conditions is plotted in. Fig. 6b. The results appear similar to those in Fig. 6a except for a small difference between water and ethanol solution at heavy preloads (≥3 mN). Fig. 6c shows the contact radius versus time during the pull-off process with various preloads in the dry case, and Fig. 6d shows the results with different wetting conditions at a constant preload of 2 mN. The key points of A, B and C are also correspondingly shown in Fig. 3. It is seen that the increased preload increases the time for keeping a constant contact radius, whereas the presence of liquids decreases that time in the pull-off process.

Fig. 7a shows the short-range dry detached force extracted from the raw force curves measured in the dry, water, and alcohol-solution cases (Fig. 3), and the long-range capillary forces surrounding the dry contact are shown in Fig. 7b. With or without liquids, the dry detached forces on soft PDMS increased slightly with increasing preload. In comparison to the dry case at the same preload, the introduction of liquid to the interfacial contact decreased the dry detached force, exhibiting a surface-tension dependence. In addition, the capillary interaction for adhesion was also heavily influenced by the surface tensions of liquids rather than the preload (Fig. 7b).

4. Discussion

4.1. Linear transition from JKR mode to Hertz mode in indentation

The edge of the contact area in adhesion can be regarded as a crack that recedes or advances following Griffith's criterion [27]. When the probe just touches the soft PDMS in indentation, the strain energy release rate G is less than the work of adhesion $\Delta\gamma$; thus, the contact edge advances, i.e., the crack recedes spontaneously in order to minimize system energy. If such an increase of contact area is quicker than the increase produced by the probe penetration, an adhesive regime would resultantly dominate the indentation (Fig. 4a).

After the adhesive regime, the correlation measured between the applied force F and press-in depth δ roughly shows a linear transition from JKR to Hertz mode with increasing load. On the contrary, the relation between applied force F and contact radius a presented in Fig. 4b is always closer to the JKR expectation. It could be a result of the viscoelastic effect induced by the structure of soft PDMS bulk, which retards the elastic response for the indentation. The JKR theory characterizes the balance between stored elastic energy U_E, potential energy U_F, and stored interfacial energy U_S for pure elastomer, which has an instant elastic response [28,29]. However, in our experiments, the specimen of soft PDMS was constituted by the crosslinked network and uncrosslinked molecules (Fig. 8a). The internal friction f induced by the segmental motion of long-chain molecules provides viscous resistance for the elastic response in soft PDMS bulk when under penetration of the probe (Fig. 8b). The strain ε lags behind the stress σ in the material [29], which may lead to a hysteretic bulk deformation, i.e., the press-in depth δ is less than the JKR expectation at the same preload F (Fig. 4a). However, such an inner hysteretic elastic response may have little effect on the surface adsorption, so the correlation of preload F and contact radius nearly agrees with the JKR mode (Fig. 4b). These suggest that the energy of viscous dissipation U_{dis} in bulk mainly expropriates the elastic energy U_E rather than stored interfacial energy U_S with the input of external work, i.e., potential energy U_F. In addition, the derivative of equation (1) with respect to time yields the expression of applied force F as follows:

$$\begin{cases} \frac{dF}{dt} = K\left(v - \frac{d\delta}{dt}\right) \\ \frac{dF}{d\delta} = K\left(\frac{v}{d\delta/dt} - 1\right) \end{cases}, \tag{4}$$

where v is the velocity of the piezo. It can be seen that the correlations of (F, δ), (F, t), and (δ, t) are coupled at the same velocity v of the piezo. Therefore, the correlation of (F, δ) in Fig. 4a can be further confirmed by the measured results of (F, t) in Fig. 2a or (δ, t) in Fig. 2b.

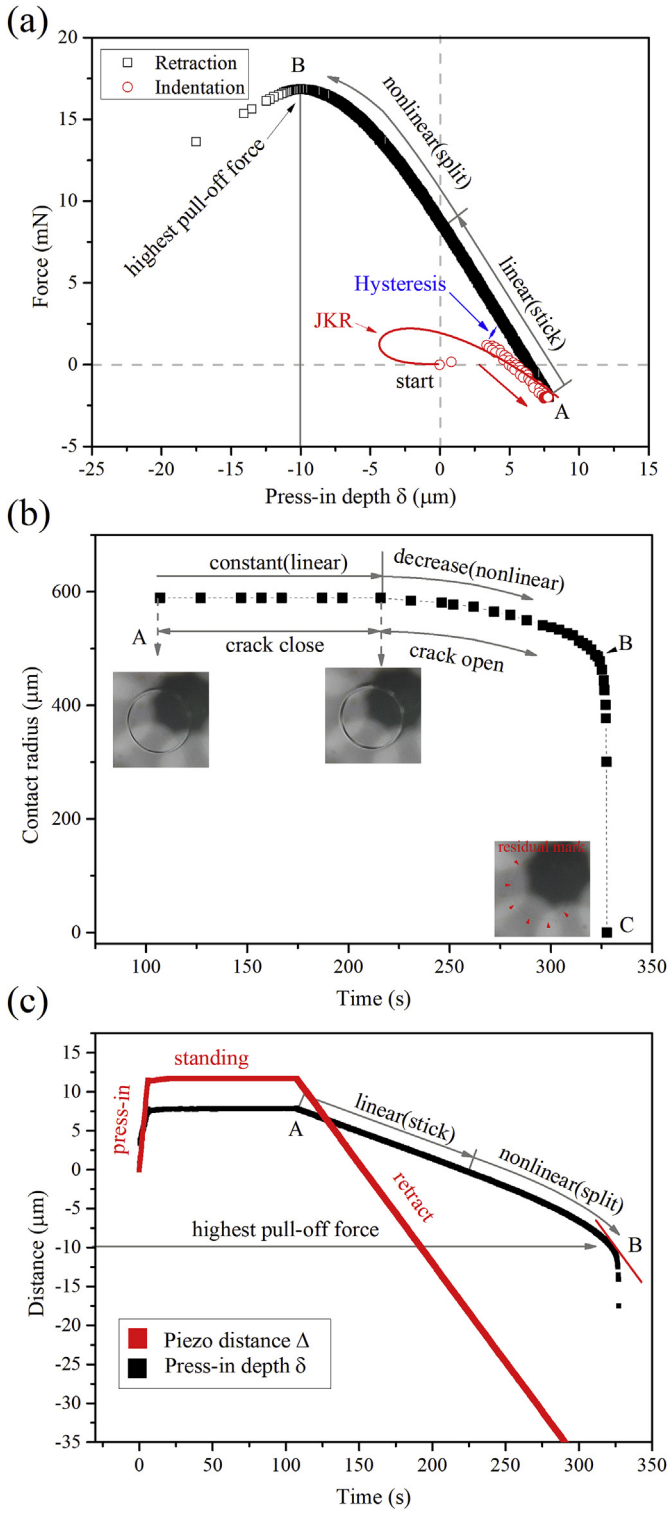

Fig. 5. Pull-off behavior between the probe and soft PDMS in the dry case: (a) The force-depth curve measured in indentation and retraction, (b) the contact radius between probe and soft PDMS versus time in retraction, and (c) the curves of piezo distance and press-in depth versus time. The velocity of the piezo for retraction was 0.25 μm/s.

4.2. Stick-split pull-off behavior in retraction

As shown in Fig. 5, the entire pull-off process on the soft PDMS surface is proposed to feature a “stick-split” behavior. In the scope of stick, the correlations of (F, δ) and (δ, t) clearly exhibit linearity; the crack of the contact edge is closed and the spherical probe performs as a flat punch, keeping the contact area constant. By contrast, in the scope of split, (F, δ) or (δ, t) exhibit a curvilinear relationship; the crack of the contact edge opens and the contact area decreases with acceleration. In these two regions, the viscous friction of segmental motion f still functions in the elastic response of soft PDMS bulk (Fig. 8d) and the strain ε and the stress σ are still out of sync, resulting in the dissipative energy of viscoelastic losses during pull-off behavior, which can be demonstrated by a residual mark on the soft PDMS after the detachments (point C of Figs. 5b and 8c). Following the crack propagation of Griffith's criterion, the stick region is configured with $G \le \Delta\gamma$; the mechanical energy dissipated by viscoelastic losses is insufficient to break through the barrier of surface energy stored in the crack tip of the contact edge. It can be described as

$$\begin{cases} U_E + U_F - U_{diss} \le U_S \\ G = G_M(F, \delta) - G_{diss} \le \Delta\gamma \end{cases} \quad (5)$$

where G_M is the original strain energy release rate and G_{diss} is the energy dissipation term. G_{diss} is attributed to slight stress relaxation and creep in dwell time of the contact [30] and the internal friction consumption in detachment.

For a pure elastomer (JKR type), after the dwell time where $G = G_M = \Delta\gamma$, the contact area decreases as soon as the probe retracts because of the increase in G [27]. For soft PDMS, our results suggest that the increase in G_M in the initial probe retraction mainly offsets G_{diss} with a fixed contact area until the case of $G = \Delta\gamma$, where the crack of the contact opens. In the split region, though the dissipative item of G_{diss} still behaves, G is sufficient to maintain the crack propagation and the excess $(G-\Delta\gamma)dA$ is changed in the kinetic energy of crack motion [9,27,31]. Compared with the JKR prediction for pure elastomer, the additional of G_{diss} can lead to an increase in G_M, resulting in a higher pull-off force F and longer stretch of the soft PDMS surface δ in the detachment [see Fig. 5a, equation (5)]. In addition, the phenomenon where the tangent line of the highest pull-off force point E is parallel to the retraction line of the piezo (Fig. 5) can be explained by equations (4) and (5). The maximum points of the (F, t) and (F, δ) functions are achieved if the stretch rate of the soft PDMS $d\delta/dt$ approaches the piezo velocity v.

4.3. Effect of wetting condition on adhesion

As suggested by Martin et al. [32], a prerequisite for the dry contact of rubber on a wet substrate is the dewetting of the intercalated liquid film (the spreading parameter $S > 0$). In our experiments, here, the dry contacts of the probe to soft PDMS are achieved in the presence of both water and ethanol solution (Fig. 3), and the work of adhesion can be expressed as [23]:

$$\Delta\gamma_l = \Delta\gamma - \gamma_l(\cos\theta_1 + \cos\theta_2) = -S, \quad (6)$$

where $\Delta\gamma_l$ is the work of adhesion of probe-PDMS in liquids, $\Delta\gamma$ is the work of adhesion of probe-PDMS in air, γ_l is the surface tension of the liquid, and θ_1 and θ_2 are the contact angles of liquid on the PDMS and probe, respectively. As with the dry case, the contact edge between the probe and PDMS in liquid advances as the crack recedes in the indentation for preload. The driving force for this advance for increasing contact area can be thereby written as

$$\Delta\gamma_l - G = \Delta\gamma - G - \gamma_l(\cos\theta_1 + \cos\theta_2) = \Delta\gamma - G - f_l \quad (7)$$

Here $f_l = \gamma_l(\cos\theta_1 + \cos\theta_2)$ is the effect of liquid on the movement of the crack of the contact edge.

Compared with the dry case of $\Delta\gamma - G$, the liquid exhibits a resistance for the advance of the contact edge if $\cos\theta_1 + \cos\theta_2 > 0$. By calculation, the f_l values for water and ethanol solution are 31.2 and 40.9 mN/m (see experimental section for contact angles and surface tensions), which behave as a resistance force for the advance of the

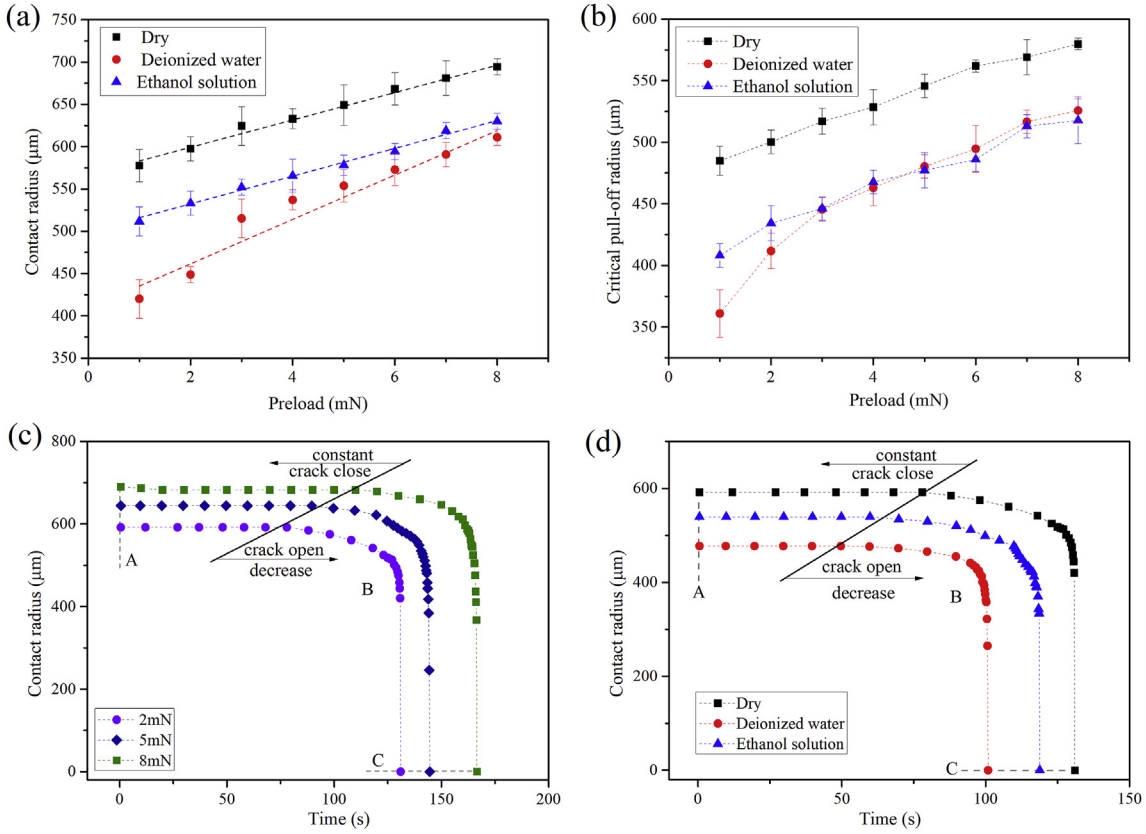

Fig. 6. (a) Contact radius and (b) critical pull-off radius dependence of preload in the dry, deionized water, and ethanol-solution cases. (c) Contact radius versus time with varying preload in the dry case, and (d) contact radius versus time in varying wetting conditions at a preload of 2 mN.

contact edge (Fig. 9). As a result, the contact area of probe-PDMS in both water and ethanol solution are inferior to that in air (Fig. 6a). Nevertheless, comparing the f_l values of water and ethanol solution shows an inconsistency to the measured results in that the contact radius in ethanol solution is greater than that in water (Fig. 6a). This is most likely due to the capillary action of liquid surrounding the contact area, which provides an additional drive on the contact edge (Fig. 9) [20,21,23]. The ethanol solution with low surface tension extends the contact edge more strongly than water because of its larger Laplace pressure.

As shown in Fig. 6c and d, the stick region of the detachment on soft PDMS can be influenced both by the preload and wetting case, but their mechanisms are different. The decrease in preload would result in a low dissipative energy of viscoelastic loss, i.e., low G_{diss}, in soft PDMS bulk, which narrows the stick region. However, for the liquid case, the primary factor is surficial liquid resistance force f_l, which decreases the critical transition point of stick-split with $G = \Delta\gamma_l = \Delta\gamma - f_l$. In comparison to the dry case ($G = \Delta\gamma$), the stick region in liquid is narrower, and the crack of the contact edge in detachment opens early (Fig. 6d).

In the split region, the nearly translational curves of Fig. 6c signify the same decreased ratio of contact radius, i.e., the velocity of crack motion in the dry, water, and ethanol-solution cases, suggesting that their changed kinetic energies $[(G - \Delta\gamma)dA$ for the dry case, $(G - \Delta\gamma_l)dA$ for liquids] were nearly the same. Thus, the difference in adhesion work ($\Delta\gamma$ or $\Delta\gamma_l$) and the critical pull-off areas (Fig. 6b) in the dry, water, and ethanol-solution cases are mainly responsible for the results of highest dry pull-off force in Fig. 7a. The higher adhesion work with the larger critical pull-off area produces a higher adhesion force. In

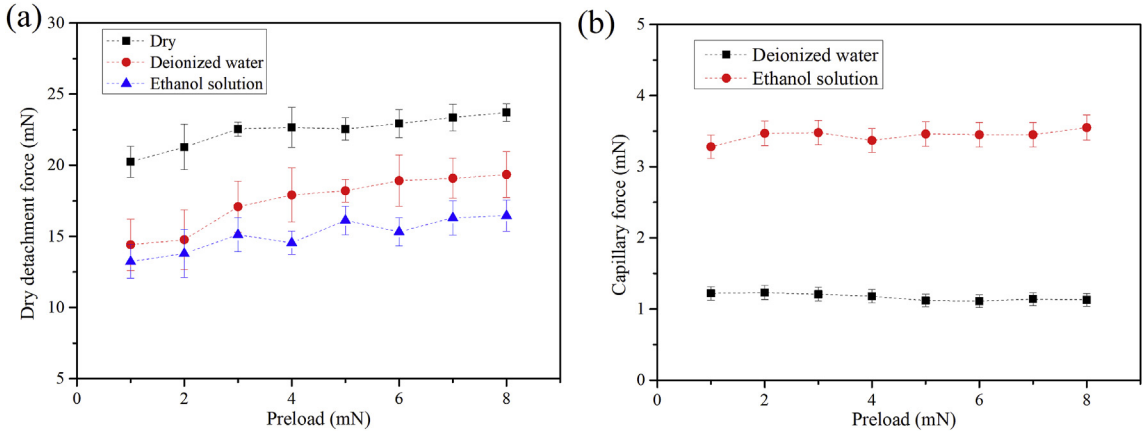

Fig. 7. (a) Dry detached force and (b) capillary force for adhesion dependence of preload in the dry, water, and alcohol-solution cases.

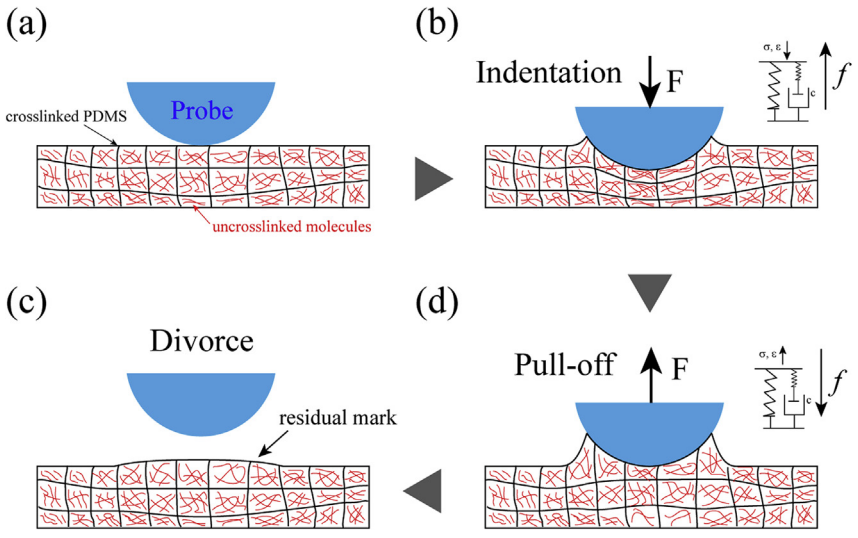

Fig. 8. Schematic of indentation, pull-off, and divorce behavior of the probe on soft PDMS.

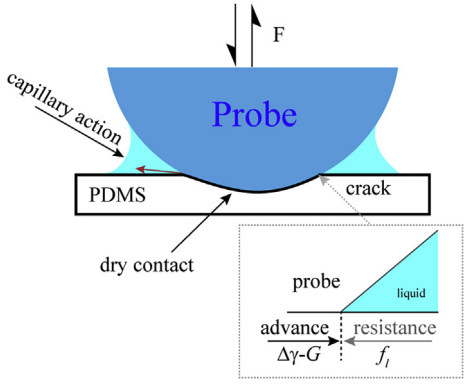

Fig. 9. Effect of liquid on the contact between the probe and soft PDMS.

addition, the higher capillary force surrounding the contact area for adhesion (Fig. 7b) is achieved by the low surface tension of the liquid because of the higher Laplace pressure.

5. Conclusions

In this study, we experimentally investigated the mechanical behaviors of the contact and adhesive of soft PDMS with a spherical glass probe in dry, deionized water, and ethanol-solution conditions. After detailed analysis and discussion, the main results and conclusions can be summarized as follows:

i. In indentation for contact, the correlation of load-penetration generally undergoes a linear transformation from JKR mode to Hertz mode with increasing preload, whereas the relation between force and contact radius is always close to the JKR expectation. The internal friction of the polymer seems mainly to resist bulk deformation, but shows little effect on the surficial adhesive contact. The energy of viscous dissipation mainly expropriates the bulk elastic energy rather than stored interfacial energy.
ii. In retraction for adhesion, a pronounced stick-split behavior characterizes the detachment because of the dissipated energy induced by bulk viscoelastic loss. For the stick region, the probe firmly sticks the soft PDMS surface without decreasing the contact area, behaving as a flat punch retracting. The highest pull-off force is achieved in the split region, where the stretch rate of soft PDMS equals the piezo speed. Both the stretch length and adhesive force of soft PDMS surface far exceed the JKR prediction because of the extra work required to compensate for the dissipated energy.
iii. Although causing additional capillary interaction for adhesion, the introduction of water and ethanol solution between the probe and soft PDMS strongly decreases the contact area, narrows the stick region, and weakens the dry adhesive strength. The reason is attributed to their positive values of $\cos\theta_1 + \cos\theta_2$, which lead to interfacial resistance to the advance of the contact edge and a reduction in the work of adhesion.

Conflicts of interest

The authors declare no competing financial interest.

Acknowledgements

This research was supported by the National Nature Science Foundation of China (NSFC) (Grant No. 51675268) and the Natural Science Foundation of Anhui Province of China (Grant No. 1708085QE113). M.L. would like to thank the China Scholarship Council (no. 201806830076) for funding.

References

[1] W.J.P. Barnes, Functional morphology and design constraints of smooth adhesive pads, MRS Bull. 32 (2007) 479–485.
[2] W.J.P. Barnes, P.J.P. Goodwyn, M. Nokhbatolfoghahai, S.N. Gorb, Elastic modulus of tree frog adhesive toe pads, J. Comp. Physiol. 197 (2011) 969–978.
[3] W. Huang, X.L. Wang, Biomimetic design of elastomer surface pattern for friction control under wet conditions, Bioinspiration Biomimetics 8 (2013) 046001.
[4] S. Wang, M. Li, W. Huang, X. Wang, Sticking/climbing ability and morphology studies of the toe pads of Chinese fire belly newt, J. Bionic Eng. 13 (2016) 115–123.
[5] A. del Campo, E. Arzt, Design parameters and current fabrication approaches for developing bioinspired dry adhesives, Macromol. Biosci. 7 (2007) 118–127.
[6] A. del Campo, C. Greiner, I. Álvarez, E. Arzt, Patterned surfaces with pillars with controlled 3D tip geometry mimicking bioattachment devices, Adv. Mater. 19 (2007) 1973–1977.
[7] D. Sameoto, C. Menon, Recent advances in the fabrication and adhesion testing of biomimetic dry adhesives, Smart Mater. Struct. 19 (2010) 103001.
[8] A.N. Gent, Adhesion of viscoelastic materials to rigid substrates. II. Tensile strength of adhesive joints, J. Polym. Sci. B Polym. Phys. 9 (1971) 659.
[9] A.N. Gent, Adhesion and strength of viscoelastic solids. Is there a relationship between adhesion and bulk properties?†, Langmuir 12 (1996) 4492–4496.
[10] M. Li, J. Xie, L. Shi, W. Huang, X. Wang, Controlling direct contact force for wet adhesion with different wedged film stabilities, J. Phys. Appl. Phys. 51 (2018) 165305.
[11] M. Li, J. Xie, Q. Dai, W. Huang, X. Wang, Effect of wetting case and softness on adhesion of bioinspired micropatterned surfaces, J. Mech. Behav. Biomed. 78 (2018) 266–272.
[12] D.M. Drotlef, L. Stepien, M. Kappl, W.J.P. Barnes, H.J. Butt, A. del Campo, Insights into the adhesive mechanisms of tree frogs using artificial mimics, Adv. Funct.

Mater. 23 (2013) 1137–1146.
[13] G.Y. Choi, A. Soojin Kim, A. Ulman, Adhesion hysteresis studies of extracted poly (dimethylsiloxane) using contact mechanics, Langmuir 13 (1997) 6333–6338.
[14] I.U. V, Akihiro Toritani, A. Masaki Nakayama, Higashitani Ko, Deformation and adhesion of elastomer microparticles evaluated by AFM, Langmuir 17 (2001) 4739–4745.
[15] U. Abusomwan, M. Sitti, Effect of retraction speed on adhesion of elastomer fibrillar structures, Appl. Phys. Lett. 101 (2012) 211907.
[16] Q. Xu, M. Li, J. Niu, Z. Xia, Dynamic enhancement in adhesion forces of micro-particles on substrates, Langmuir 29 (2013) 13743–13749.
[17] G. Castellanos, E. Arzt, M. Kamperman, Effect of viscoelasticity on adhesion of bioinspired micropatterned epoxy surfaces, Langmuir 27 (2011) 7752–7759.
[18] V. Barreau, D. Yu, R. Hensel, E. Arzt, Elevated temperature adhesion of bioinspired polymeric micropatterns to glass, J. Mech. Behav. Biomed. Mater. 76 (2017) 110–118.
[19] F. Wu-Bavouzet, J. Clain-Burckbuchler, A. Buguin, P.G. De Gennes, F. Brochard-Wyart, Stick-slip: wet versus dry, J. Adhes. 83 (2007) 761–784.
[20] D. Xu, K.M. Liechti, K. Ravi-Chandar, On the modified Tabor parameter for the JKR–DMT transition in the presence of a liquid meniscus, J. Colloid Interface Sci. 315 (2007) 772–785.
[21] D. Maugis, B. Gauthier-Manuel, JKR-DMT transition in the presence of a liquid meniscus, J. Adhes. Sci. Technol. 8 (1994) 1311–1322.
[22] P. Martin, Adhesion of a soft rubber on a wet solid, J. Adhes. 67 (1998) 139–151.
[23] J. Qian, J. Lin, M. Shi, Combined dry and wet adhesion between a particle and an elastic substrate, J. Colloid Interface Sci. 483 (2016) 321–333.
[24] M. Li, W. Huang, X. Wang, Advanced adhesion and friction measurement system, Meas. Sci. Technol. 28 (2017) 035601.
[25] V.L. Popov, Contact Mechanics and Friction: Physical Principles and Applications, Springer Berlin Heidelberg, 2010.
[26] D. Maugis, Contact, Adhesion and Rupture of Elastic Solids, Springer Science & Business Media, 2000.
[27] D. Maugis, Fracture mechanics and the adherence of viscoelastic bodies, Journal of Physics D-applied Physics 11 (1978) 1989.
[28] K. Johnson, K. Kendall, A. Roberts, Surface energy and the contact of elastic solids, Proceedings of the royal society of London. A. mathematical and physical sciences 324 (1971) 301–313.
[29] M.T. Shaw, W.J. Macknight, Introduction to Polymer Viscoelasticity, third ed., Wiley, 1983.
[30] Renato Buzio, Alessandro Bosca, Silke Krol, Diego Marchetto, A. Sergio Valeri, U. Valbusa, Deformation and adhesion of elastomer poly(dimethylsiloxane) colloidal AFM probes, Langmuir 23 (2007) 9293–9302.
[31] M.K. Chaudhury, Rate-dependent fracture at adhesive interface, J. Phys. Chem. B 103 (1999) 6562–6566.
[32] P. Martin, F. Brochard-Wyart, Dewetting at soft interfaces, Phys. Rev. Lett. 80 (1998) 3296–3299.